Journal of Electronic Materials (2021) 50:5090–5105
https://doi.org/10.1007/s11664-021-09079-0

TOPICAL COLLECTION: CARBON-BASED MATERIALS FOR ENERGY STORAGE

Graphene for Thermal Storage Applications: Characterization, Simulation and Modelling

Dhinakaran Veeman[1] · M. Swapna Sai[1] · V Rajkumar[2] · M. Ravichandran[3] · S. Manivannan[4]

Received: 2 January 2021 / Accepted: 21 June 2021 / Published online: 12 July 2021

Abstract

In recent years, interest in the thermal properties of graphene constituents has seen rapid growth in the fields of science and engineering. The removal of heat in the continuous processes in the electronics industry has had major issues in thermal transmission in lower-dimensional assemblies. It has also shown fascinating topographies as the carbon allotropes and their derivative compounds expel heat. Numerous research articles reported within the past 15 years have demonstrated enhanced electron flexibility, exceptional thermal conductivity and mechanical behaviour, as well as excellent optical properties of graphene as a single atomic layer. This review article tries to provide a detailed summary of the heat exchange properties of graphene structures and graphene-based materials such as nanoribbons with few-layered graphene. Thermal and energy storage management systems have played a major role in the increase in marketable products in recent times. The purpose of this review is to summarize the current research on thermal properties with regard to the management and energy storage of graphene materials, focusing on characteristic properties, industrialization, modelling and simulation, and their applications in specific thermal storage systems.

Keywords Graphene · thermal storage · energy · thermal devices · PCM

Introduction

A typical problem faced by large energy storage and heat exchange system industries is the dissipation of thermal energy. Management of thermal energy is difficult because the concentrated heat density in electronic systems is not experimental.[1] The great challenge of heat dissipation systems in electronic industries is that the high performance in integrated circuits significantly increases the power consumption. In recent times, Moore's law has not been in use, as the physical conditions and limitations imposed on quantum effects is minimized.[2]

✉ Dhinakaran Veeman
dhinakaranv@citchennai.net

[1] Centre for Applied Research, Chennai Institute of Technology, Chennai, Tamil Nadu, India

[2] Department of Mechanical Engineering, PSG Institute of Technology and Applied Research, Coimbatore, Tamil Nadu, India

[3] Department of Mechanical Engineering, K. Ramakrishnan College of Engineering, Trichy, Tamil Nadu, India

[4] Department of Mechanical Engineering, Karpagam Academy of Higher Education, Coimbatore, Tamil Nadu, India

Graphene materials are emerging as the latest methodology to store energy, and the use of transistors is decreasing, as it is likely to impose tension on the thermal management systems without the inclusion of non-uniform heating between chips.[3] The two-dimensional (2D) materials are layered structures with firm thickness which bond to a hexagonal carbon lattice plane and display good operational, electric, current and mechanical properties, and as a result, these materials have become one of the foremost materials in research fields to employ it in numerous applications of science and engineering.[4] Figure 1 shows the measurement of heat conduction by utilizing a graphene structure. Graphene was heated with a laser light concentrated in the centre of the suspended part. The temperature increase is determined by changing the position of the G peak in the Raman spectrum of graphene. The exceptional properties of graphene and 2D materials have made it possible to employ them in various electronic systems such as batteries, sports equipment, and solar cells, and they have great potential impact in future applications as well. The enhanced thermal conductivity of graphene and 2D-based materials has made them uniquely suited for the direct thermal management and control of electronic systems.[5] The extensive wavelength phonon transport in 2D crystal lattices makes

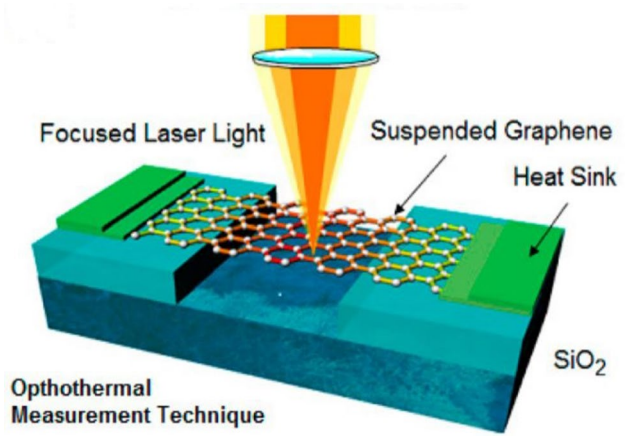

Fig. 1 Schematic of graphene structure used for the measurement of thermal conductivity. Reprinted from Ref. 6, under the terms of the Creative Commons Attribution License CC by 4.0 licence, https://creativecommons.org/licenses/by/4.0/.

graphene-based materials the strongest with an exceptionally long free path limited by sample size despite deviations of heat transfer.[7] Widespread studies have been carried out using by-products of graphene such as graphene oxide (GO), graphene film, graphene fiber, graphene foam, graphene laminate, and graphene thermal interface materials (TIMs) for heat administration applications along with the exceptional thermal properties of graphene structures and graphene-based materials.[8] Graphene also serves as a strong thermal alloy filler substance rather than carbon nanotubes (CNT) owing to its exceptional thermal requisite property and its inexpensive conditions. The patterned graphene layer films, fabricated from graphene flake layers, display outstanding thermal functioning and enhanced efficiency as heat dissipaters.[9] This mini review article explores the recent developments in thermal management systems using graphene and graphene-based materials along with other 2D materials which include hexagonal boron nitride (HBN).[10,11] Overall, the variation in thermal modelling methods applicable to these graphene materials are obtainable with the view of modelling and simulation in various thermal management systems and energy storage devices. They are summarized and described with parameters and accuracy, and lastly, the major problems and potential uses of graphene materials and other 2D materials for thermal and energy storage systems are discussed in detail.

Stimulation of Graphene Materials in Thermal Engineering

Graphite is a form of naturally occurring carbon. It is, opaque, black to steel grey, and has a soft lubricating texture. Graphite shows two crystalline structures, hexagonal and rhombohedral. Both crystalline structures have high anisotropy levels that determine the characteristics of graphite, particularly electrical and mechanical. Graphite is recognized as a superior heat and electricity driver, for its maximum natural strength and rigidity over other minerals, its resistance to chemical attacks and its resistance to temperatures higher than 3600 °C (6500 °F). Graphene is a pure type of carbon in which each particle can be accessed from different sides for fabrication response. Particles on the edges of a sheet of graphene are unique in chemicals. It has the highest percentage of edge atoms. Impurities in a graphene sheet increase the reactivity of the substance. Its thermal conductivity and mechanical strength result in the good in-plan characteristics of graphite (independently around 3000 W m^{-1} K^{-1} and 1060 GPa), and its breakdown quality is comparable to that of carbon nanotubes, for virtually the same kind of defects. Graphene can produce next-generation electronics, biomedical products, composites and coating, sensors, and membranes that are currently limited, and manufacture them faster with a wide range of outstanding qualities. The production of enhanced source density batteries such as lithium-ion (Li-ion) batteries has made progress in the usage of cell phones, personal electronics and motorized industries, as the temperature increase outside the usual operating range has a negative impact on the effectiveness of the Li-ion batteries, and if overheated, the battery causes the cell to split or burst.[12] The thermal phase change material (PCM) can predict heat control of high-density ion battery packs, which in turn minimizes the temperature increase in the battery owing to concealed heat storage and segment variations over a minimum temperature range.[13] Typically, PCMs have much lower thermal conductivity, in the range of 0.17–0.35 W m^{-1} K^{-1} at room temperature, compared with the heat conduction of silicon (Si) and copper (Cu) at room temperature (RT), which lie in the range of ~145 W m^{-1} K^{-1} and ~381 W m^{-1} K^{-1}, respectively.[14] Figure 2 shows graphene-based material used as a thermal device under coupling quantities. Thermal devices are classified according to their physical dimensions, which can be mainly divided into four categories: uncoupled thermal devices, thermoacoustic coupling devices, thermoelectric and thermo-optic coupling devices, and various functional devices. The predicted PCMs store heat from the battery as a replacement for heat transfer to the battery pack. They are also employed in battery cells to shield the battery-operated cell from large ambient temperature variations which completely differs from the heat regulation of processor coded chips.[16] In order to minimize the temperature range, the device uses chip surge, thermal interface material (TIM) or heat propagators to allow the transfer of heat from the defect to the heat sink.[17] The heat conduction of TIM is in the range of about 1–10 W m^{-1} K^{-1}, while the thermal diffusion of solid graphite-based materials is in the range of 1000 W m^{-1} K^{-1}.[18] The graphene material serves as a filler

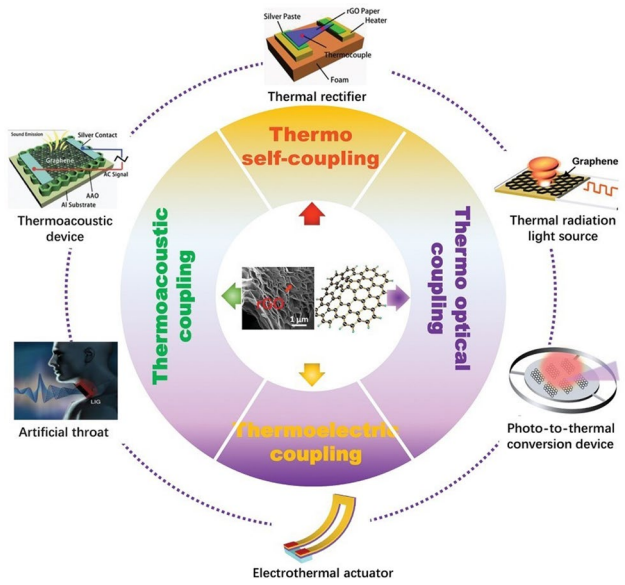

Fig. 2 Thermal devices of graphene material under coupling quantities. Adapted with permission from Ref. 15, Copyright 2019, John Wiley and Son.

for thermal conductivity by introducing in the current analysis a hybrid PCM of these two separate thermal management methods.[19] The properties that make graphene an extraordinary filler material are its enhanced internal heat conduction and durable bonding to numerous matrix materials.[20]

Thermal Conductivity of Graphene

Heat transfer is slowed by the impact of microscopic elements along with the amount of heat carrier charges in the area. The thermal performance is controlled by Fourier's law, which is expressed as:

$$q = -k \cdot \Delta T \tag{1}$$

q, the limited temperature flux has units of W m^{-2}, the heat conduction of the substance has units of W m^{-1} K^{-1} and the limited temperature increase has units of K m^{-1} , which is the heat conduction of the substance.[21] Fourier's law elucidates the heat flow from a high-temperature section to a lower-temperature section, and it can be precisely calculated in a substance. However, in electronic systems the thermal conduction of heat has to be supported over various materials by exchange interfaces, and thermal resistance is widely used to regulate the ability of heat carrier transport as it is stabilized and relaxed. The thermal resistance is:[22]

$$R = \Delta T/Q \tag{2}$$

ΔT is the temperature variance (K) and Q is the heat energy (W) of the outer binary surfaces.[23] The entire heat resistance (R) comprises the heat resistance of the materials laterally. The temperature conduction path is determined by the heat conduction and depth of the materials along with the exchange at the interface of two dissimilar materials, based on numerous features including the bonding strength of materials, surface roughness, and surface cleanliness, among many others.[24]

In optical performance, the ΔP heater is furnished with an optical laser light focussed on a deferred graphene layer associated with the heat sink at both corners. The temperature increase ΔT, in response to the degenerated power ΔP, is studied by Raman spectroscopy.[25] The Raman G peak in the graphene spectrum revealed the enhanced temperature, T, dependence. Standardization of the spectral position of the G peak at temperature must be done by altering the heat using a lower laser power source in order to avoid limited heating.[26] The deferred graphene layer is heated by growing laser power through thermal conductivity dimensions. The limited temperature increase of graphene is given by $\Delta T = \Delta\omega G/\varphi G$, where φG is the heat coefficient of the Raman G peak in the suitable temperature range.[27]

Thermal Conductivity of Graphene Materials

The unusual thermal conductivity characteristics of graphene have led to further investigations of graphene materials and few-layer graphene (FLG) in TIM, thermal compounds and coverings.[28] In the first study of graphene alloys, smaller freight segments of arbitrary graphene fillers increased the thermal conductivity of epoxy alloys.[29] Various types of graphene thermal alloy fabrication methods are derived from variations in matrix material, graphene efficiency, lateral size and thickness of the graphene filler, and other types of thermal conductivity.[30] Most of the preliminary studies of graphene filler thermal alloys were restricted to the lower loading fractions of the filler, $f < 10$ vol.%. These conditions recently changed when large graphene loading compounds became available due to technical developments and substantial cost reductions.[31] The thermal properties of alloys with a high loading fraction of graphene or FLG fillers are of interest from the point of view of basic science and practical applications. Higher loading results in thermal percolation in alloys.[32] Thermal percolation is a process which is not well understood as electrical holes. An electrical hole is designated by the scaling law, where the electrical conduction of the alloy, the freight capacity portion of the filler, the loading fraction of the filler and the critical exponential are within the electrical charge limit.[33] Figure 3 depicts the heat dissipation of a graphene-based epoxy composite. In most cases, as opposed to electrical conductivity, thermal

conductivity of alloys does not show any visible fluctuations. To overcome the complex of nanofillers in the polymer, their applications improve the thermal conductivity of the mixture, in which case graphene is enhanced by the chemical vapour deposition on the foam. Further production of graphene thermal composites face issues such as hexagonal boron nitride (HBN) control of electrical and thermal separation in graphene alloys with filler optimization and combination of graphene and other electronic 2D insulation fillers.[34] In addition, graphene composite materials have shown that they are good prospects as heat sink materials.[35] Possible heat sinks are made of metal, such as copper or aluminium, with wings to raise the surface area. However, because of its low weight, anisotropy and higher thermal conductivity, carbon-based heat sink structures are of much interest.[36] Graphite has a long history and is known to be a material for heat sinks. In recent years, patents have been filed on the basis of graphene-improved heat sinks due to the benefits of lower weight and higher heat efficiency.[37] In addition, graphene or graphite-based materials for heat sinks can control thermal conductivity in different directions, allowing for preferential heat transfer.[38,39] Some of the reported works about graphene and graphene polymer composites include electromagnetic pollution, which is damaging to human health and interferes with the normal operation of other electronic equipment, is also becoming increasingly serious as miniaturization, densification, and high-power electronic products are rapidly evolving. By absorbing electromagnetic energy and converting into heat energy, it can be effectively reduced, leading to another problem when temperatures increase. There is therefore urgent theoretical significance and potential practical application for the design of polymer composites with a high thermal conductivity (λ) coefficient and outstanding electromagnetic interference shielding effectiveness (EMI SE). The λ value of epoxy nanocomposites reaches a maximum 2.3 times higher than pure epoxy resin.[40] The resulting problem has gained prominence over thermal dissipation, which has greatly affected the stability and service life of the products produced. Preparation of materials with a high coefficient of thermal conductivity (λ) is an important solution.[41,42] An efficient and cost-effective method is to introduce highly thermally conductive composite compounds in order to improve the final λ values of polymers. Excessively high loads of thermally conductive fillers are often in demand, however, to achieve relatively high λ, posing significant problems such as poor treatment, degraded mechanical characteristics, increased density and cost.[43] This is followed by a combined method of in situ polymerization, spinning and hot pressing, to produce the corresponding thermally superior nanocomposite polyimide. In view of the filler or matrix interfaces, filler dispersion and alignment, an improved thermal drive model is also proposed and established.[44]

3D Structures of Graphene Materials

Graphene Foam

Graphene foam comprises graphene structures packaged in a permeable macroscale foam structure. The foam absorbency substantially decreases the actual thermal conductivity of graphene foam, with thermal conductivity varying from 0.26 W m^{-1} K^{-1} to 1.7 W m^{-1} K^{-1} at 0.45 vol.% of solid density.[46] However, thermal conductivity of graphene foams is similar to the volume of metal, which has a high absorbency. In accumulation, graphene foam has the highest grade of compression, making it desirable for TIM applications.[47] Graphene foam is principally fabricated by graphene chemical vapour deposition (CVD) in Ni foam and then leaves the free-graphene structure by engraving the prototype. Similar construction may also be achieved by the use of a restriction moulding or a hydrothermal decrease of the GO suspension.[48] As stand-alone assemblies, both graphene material foam or graphene CNT air gel are shown for TIM applications with a heat conductivity of about 88 W K^{-1} for low graphene foam and lower thermal interface resistance at low pressure. Analogous assemblies have been

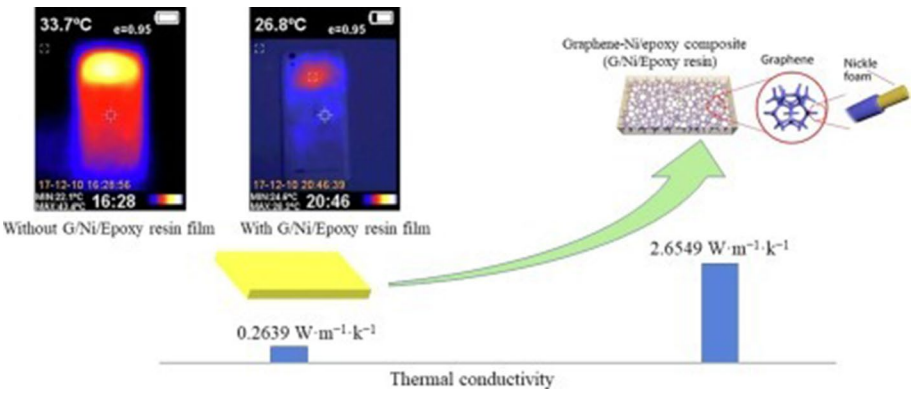

Fig. 3 Schematic of heat dissipation of epoxy composite. Reprinted from Ref. 45, under the terms of the Creative Commons CC-BY-NC-ND 4.0, https://creativecommons.org/licenses/by-nc-nd/4.0/.

confirmed using h-BN with cross-plane heat conductivity up to 62 W m^{-1} K^{-1} for flattened h-BN foam.[49] Graphene and h-BN foam penetrate to form polymer composites. Another vertically oriented graphene foam epoxy complex is formed with a flat-to-thermal conductivity of 35.5 W m^{-1} K^{-1} at 19% graphene loading fraction, which is much higher than the randomly distributed graphene improved composites. Thus, graphene-carbon hybrid foam is demonstrated to be a good candidate as a thermal basin.[50]

Perpendicular Arrangement of Graphene Sheets

Graphene slip materials have an exceptional level of thermal conductivity; nevertheless, they are usually unfit for heat dissipation applications owing to their poor level of thermal conductivity.[51] A possible resolution for this limitation is to stack several graphene sheet structures to make a weight substantial enough that it can be employed for TIM and further thermal applications. Liang et al. studied the idea of producing a material with isothermal conductivity of 112 W m^{-1} K^{-1}. Graphene film is soldered and combined with joints or silicone, and then the thermal conduction axis is applied diagonally to thin slices.[52] This principle was improved at 615 W m^{-1} K^{-1} and 1379 W m^{-1} K^{-1}, with thermal conductivity, proposed by Wong et al., which eliminates typical TIM defects with unusually high thermal conductivity compared to traditional TIMs and a thicker bond line than the heat sink material [reference]. Figure 4 explains the stepwise process involved in a 3D graphene film composite. An aqueous mixture of PS nanospheres and CMG sheets was filtered to obtain porous chemically modified graphene (CMG) film with a uniform pore size of 2 µm, followed by removal of polystyrene (PS). As a replacement for conventional Thermal interface materials (TIMs), the thermal resistance between the TIM and the bonding exteriors limits the thermal conductivity factors.[53] As Wong et al. and others have noted, overall performance depends primarily on contact, and retaining performance rivals, good ductility and thickness by bonding to a thin indium layer with thin solder joints is critical for slit satisfying applications.[54]

Graphene Hybrid Assemblies

The unique properties of 2D graphene materials can be combined and exploited in conjunction with other hybrid materials. In general, the thermal conductivity of graphene structures through the plane is a limitation.[55] One way to improve Z-directional thermal conductivity is to add further heat paths over the covalent bonding nature of the graphene material layers using intermediate content. Figure 5 shows the self-assembly of graphene-based hybrid film coating the surface., with graphene single-phase self-assembly on the copper heating surface. At the time of heating, the graphene oxide sheet is dispersed in the solution and reduces conventionally and accumulates on the heating surface by the nucleation of the vapour bubbles and creates a well-ordered graphene network. Carbon nanorods and recently used SiC nanorods have been shown to be vertically aligned in situ.[56] With this method, the thermal conductivity in the TIM application is increased from 4 W m^{-1} K^{-1} to 17 W m^{-1} K^{-1}. Hybrid graphene structures or CNT assemblies with increased CNT arrangements on graphene film can be employed for effective thermal degeneracy or new TIM assemblies[57] (Table I).

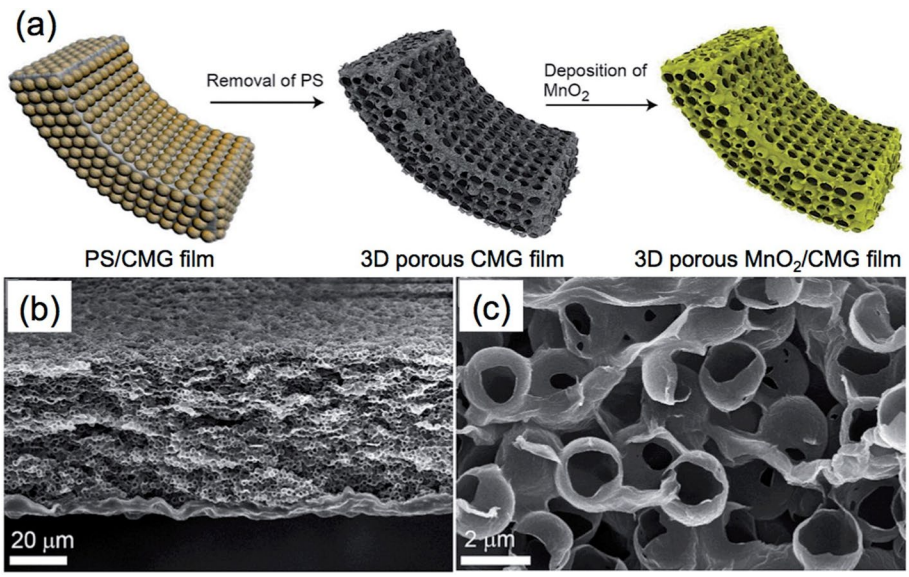

Fig. 4 The synthesis process of 3D graphene composite film. Reprinted from Ref. 50, under the terms of the Creative Commons Attribution License CC-BY-NC 3.0 Unported, https://creativecommons.org/licenses/by-nc/3.0/.

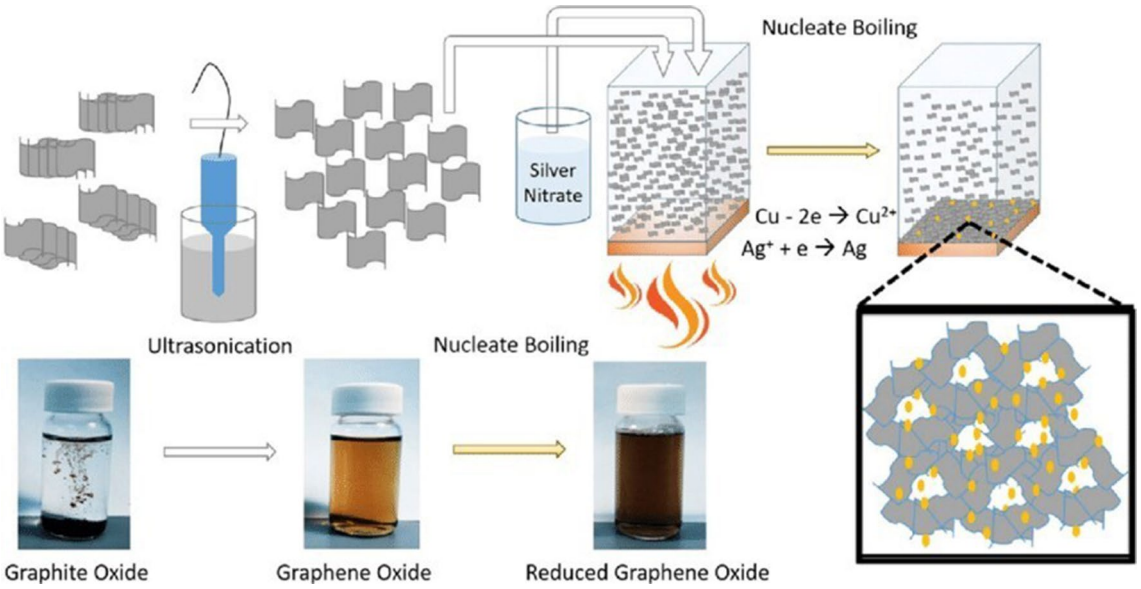

Fig. 5 Self-assembly of graphene hybrid layer coating. Reprinted from Ref. 58, under the terms of the Creative Commons Attribution License CC-BY 4.0, https://creativecommons.org/licenses/by/4.0/.

Modelling of Heat Transfer in Graphene

As the most abundant material, carbon is frequently used in fields such as electrical equipment and energy storage systems, as graphite is considered as the basic brick material of graphene modelling.[64] The advanced graphene modelling techniques diminish the conventional methods and computing theory density of binding models which includes structures for quantum description, electronic properties with their by-products and chemical mixtures which are inadequate to zero temperature range and they encompass in small dimensions in consumption.[65] The late emerging materials such as fullerenes and graphene-based materials and the nanophysics assemblies are considered with their thermal properties of graphene by utilizing molecular kinetic methods. The molecular subtleness is a scientific approach method of atomic motion based on a non-biased clarification of energy domain and the intersonic powers designates the foremost heat transporters.[66] The thermal regulation of nanodevices is achieved efficaciously by accurate amalgamation of graphene-based materials and alloys and their thermal properties are studied when they are in direct contact with the surface and at the same time when contact is active in nature.[67]

Modelling-Based Optimization of Thermal Organization with Graphene-Improved PCM

It provides useful knowledge for computer modelling materials and device optimization of battery pack thermal control systems. We have described our experimental findings from a theoretical resolution as well-defined by the thermal dispersal comparison for temporary heat transmission in the parametric data of solid and transparent battery-operated models.[68] The limitations, laterally with the restrained factual temperature and thermal conductivity properties of the

Table I Comparison between material fabrication process and graphene materials.[59–63]

Material structures	Raw material	Dispersion method	Film method	Heat treatment	Thermal conductivity ($Wm^{-1}k^{-1}$)
Graphene film	GO	Ultrasonication	Vacuum filtration	1200	1043.5
Graphene film	GO	Ultrasonication	Self-assembly	2000	1100
Graphene film	Graphene	Ball-milling	Vacuum filtration	2850	1434
Graphene film	Graphene	Ultrasonication	Electro-spray deposition	2850	1434
Graphene film	GO	Shear mixing	Self-assembly	2850	3214

adhesive compounds, were utilized in the simulation of conductive heat fluxes in Lithium-ion battery packs using the COMSOL processor simulation package kit.[69] The built-in three-dimensional (3D) model leads to the study of six-cylinder battery-operated packs in dissimilar media. Six batteries, 18.4 mm in diameter, are consistently disseminated in a solid, 70 mm in diameter, all of which are housed within a 1 mm thick aluminium covering.[70] Owing to the basic nature of the battery pack, an additional dense mesh of free tetrahedral was utilized for stable cylinders with a heat transfer intermediate linked to the rigid cylinders and the aluminium sheath.[71] The temporary heat transmission comparison has been resolved to regulate the temperature increase within the external battery pack. In all simulations, only the physical properties of the intermediate run change the interplanetary between the battery cylinders.[68] Various media including air, traditional PCM paraffin and graphene-based materials are enhanced with PCM. For traditional PCM paraffin oil deprived of graphene structure, the usage of thermal conductivity at $K = 0.25$ W m^{-1} K^{-1}, mass density of about 900 kg m^{-3} and thermal efficiency ranging at 2500 J kg^{-1} K^{-1}. The simulation effects provide continuous temperature and time measurement for a single point within a 3D modelling battery-operated packet at any given period.[72] The exact positions of the statistics were evaluated according to the corporal location of the thermo column in the empiric test rig. These simulation findings were compared to the empiric evidence of thermocouples.[73] The maximum temperature ranges of the cylinder decrease to 320 K with the traditional paraffin PCM medium. The best efficiency of these battery cylinders, however, is the amalgam graphene PCM material medium heat control with a determined temperature of about 310–315 K. is the more stable temperature outline.[74] It must be remembered here that even at small graphene loading fractions, a major reduction in the temperature of the battery-operated cylinder is accomplished.[75]

Molecular Dynamics Mimics the Interfacial Thermal Resistance Associated with Graphene

Considering and managing interfacial heat resistance with certain graphene structures and graphene layers is critical for the creation and display of FLG-based graphene layer films in heat organization. Many factors control the interfacial thermal resistance of graphene, which is dependent on the number of layers, the surface properties, and the interfacial connection.[76] Figure 6 shows the tensile test performance of graphene using the FLG model. FLG was prepared by applying graphene layers by maintaining a distance of 3.4 Å between them. In this section, we discuss the development of graphene-based interfacial thermal resistance in molecular dynamics, with the goal of delivering a good representation of how these main variables influence the thermal properties of the interface.[77]

Influence of Number of Graphene Layers

The number of graphene layers has a direct influence on the internal layer thermal resistance of some graphene layers as well as the resistance between the FLG layers and the substrate.[78] Owing to the investigational imprecision, it is problematic to calculate the numeral persuaded layer heterogeneity of heat resistance unwavering from traditional tentative methods. Providentially, supercomputer simulations such as molecular subtleties offer a precise and quick approach to address these challenges.[79]

Inter-layer Thermal Resistance Depending on the Number of Layers in Graphene

Using non-equilibrium molecular dynamics (NEMD) simulation software, Wei et al. measured the layered based interfacial thermal resistance between binary coupled graphene layers where R_{inter} thermal resistance was attained.[81]

$$(N-1)\cdot R_{\text{inter}} = N\cdot L/K_c \tag{3}$$

L is the depth of the layer (0.34 nm), N is the number of layers and K_c is the operative cross-plane thermal conductivity of multilayer graphene. The rate of the interfacial thermal resistance for $N = 48$ is an order of magnitude less than $N = 6$. It is a hot and cold reservoir that limits the average free path of the phonon, which induces intercontinental thermal resistance and simply decreases with layer number.[82] Ni et al. used a method based on the molecular dynamics of equilibrium (EMD) simulations to eliminate the effect of size in NEMD. The thermal resistance between two structures with a temperature difference between T can

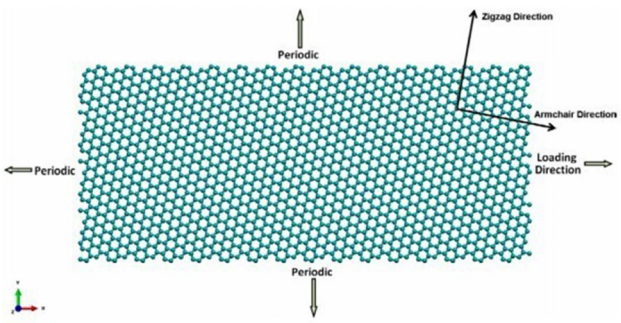

Fig. 6 FLG model for performance of tensile test using graphene. Reprinted with permission from Ref. 80, Copyright 2011, Elsevier.

be determined using the following equation suggested by R_{int} Volz et al.

$$R_{\text{int}}K_{\text{B}} = \int \{T\,(0)\,\Delta T(t)\}/\left\{T\,(0)^2\right\}\,\mathrm{d}t\,(1/N_1 + 1/N_2) \tag{4}$$

If K_B is the Boltzmann constant, then n_1 and n_2 apply to the number of degrees of freedom between the two subsystems. This procedure is non limited to heat sinks and can be used to measure the thermal resistance between two identical coatings of graphene.[83] Resistance measured in different ways confirms that as the amount of FLG increases, the resistance to interference decreases. Lastly, the interfacial resistance exceeds the graphite boundary with a large number of layers.[84]

Coating Layer Number-Based Interfacial Heat Resistance Between Some Layered Graphene and One Surface

The heat system relationship between the graphene materials and the surface is characterized by the contact angles of van Der Waals interactions, while a significant number of studies have been performed on single-layer graphene (SLG) substrate and FLG–substrate interaction resistance. SLG-substrate contact resistance is often believed to be independent of layer number because there is no association between resistance and coating number owing to investigational imprecision.[85] Though, molecular dynamic balance controls indicate that the touch resistance between FLG and SiO_2 reduces with the number of layers and congregates for six graphene structure layers, suggesting that the results are in reasonable arrangement with the investigational standards.[86] For FLG with one to four coating layers, with more than four layers, the calculation provides a variety of resistance owing to minimal untried precision, whereas the mean rate is $2 * 10^{-8}\ m^2\ KW^{-1}$ similar to $1.7 * 10^{-8}\ m^2\ KW^{-1}$.

Outcome of Intraocular Coupling and Surface Properties

Intracellular thermal resistance between the graphene or FLG graphene layer and substrate is a major limitation of their thermal efficiency in devices.[87] The covalent molecule has been shown to successfully facilitate the flow of heat between the interfaces by adding additional heat pathways across the molecule. Research on the thermal efficiency of a graphene film is aided by the inclusion of silicone-functional molecules.[88] The calculations of their molecular subtleties demonstrate that the equivalent thermal conductivity and the thickness of the silane-based particles decrease.[89] Wang et al. stated that interglacial heat transfer engineering can be achieved by interaction with the host organ, such as the organ that governs interfacial thermal conductivity, and by electronically isolating the assisted graphene layer.[90] Luo et al. used NEMD constant-state to measure the graphs interfacial thermal resistance of graphene material or graphite-polymer systems. Graphene originates that longer wavelength photons in graphene play an important role in the flow of heat through the polymer interface.[91] The presence of lower-frequency methods of about 2–16 Hz owing to vibrations beyond the aircraft makes for a good mixture of graphene ranges and polymer spectra, thereby enabling interfacial heat transfer.[92] Using molecular dynamics (MD) simulations, Chen et al. reported that FLG thermal conductivity increases exponentially with the thickness of the sheet, exceeding 90% of the bulk graphite cap at six coatings and finally at 13.4 nm (40 layers). With the NEMD simulation, Li et al. analysed the crystallization consequence of the silicon carbide (SiC) surface and observed that the amorphous interface was less than the Rint sparkling interface.[93] This effect is due to the uneven external characteristic of the amorphous artifacts and the large photon channel unlocked by the soft photon thickness of the amorphous SiC states.[94] However, Zhang et al. reported that the thermal dissipation performance of a 2D junction transistor is strongly dependent on the heat conductivity of the surface and that it is problematic to decrease the temperature of the hotspot by changing the resistance of the 2D material substrate boundary.[95,96] In addition to the reasons described above, the thermal properties of graphene materials are often influenced by other methods, such as strain engineering and the manufacture of phonetic crystal structures.[97]

Consequence of Doping on Graphene Thermal Performance

Doping is excellent method to expose a large and tidy doping tune. The doping elements boron (B) and nitrogen (N) atoms are common contenders for doping in graphene, the equivalent molecular size of carbon (C) and their pore receptors, and the position of the electron donor in computing B- and N-doping, correspondingly.[98] However, doping influences the heat efficiency of graphene. Shi et al. studied the interfacial thermal tolerance and thermal enhancement of nitrogen-doped zigzag graphene (NDZG) using NEMD. Intercellular thermal resistance in place of nitrogen doping has been shown to induce a sharp decrease in heat conduction of NDZG.[99] Thermal correction of trivalent single-nitrogen doped graphene (SNDG) with increasing temperature. Defects of varying relations on the thermal conductivity of graphene and the effects of isotopic doping were studied by Chen et al., in which spectral photon refers to the lessening period and the standardized accumulated heat conduction of the free path photon, suggesting that extended mean free path (MFP) phonon modes are firmly repressed in deficient and incapacitated graphene, leading to repressed volume dependency and weakened temperature dependency of heat conductivity relative to ancient graphene materials.[100,101]

Graphene Works to Increase Heat-Dissipating Performance

Graphene in plain thermal transference can be improved by increasing the biochemical bond between the graphene and the surface.[102] The thermal control of the micro-heaters is thus significantly enhanced by the incorporation of alternate heat-dispersed channels by aminosilane molecules that are coated with functionalized graphene oxide (FGO) attached to the graphene film assembly (GF).[103] The GF is bound to the surface of the FGO by aminosilane molecules such as (3-aminopropyl)triethoxysilane (APTES) which contains the three-O-group and has the NH_2 end due to the general chemistry of APTES, which readily binds to two dissimilar surfaces.[104] The Si-O termination of the APTES is attached to the GO surface and the cross-linked Si-O assembly serves as a solid supplementary coating between the surface and the GF with the azanide (NH_2) end of APTES binds to the carboxyl groups of the functionalized graphene film.[105] The microscopic cause of improvement of thermal conductivity (k) in graphene film was examined by mode-based analysis of the photon reduction time through the addition of the APTES molecule, and the reducing period of the acoustic flexural mode plane mode (ZA) is greatly increased at lower frequency curves; however, the longitudinal and transverse modes are marginally diminished.[106] ZA mode refers to the increase of k of the graphene layer film bound to the surface of ZA mode when it contributes more than 77% to 300 K. Molecular dynamic simulations and abiotic measurements demonstrate that there is an error in the function.[107] Figure 7 shows the graphene film applications as a heat spreader. The high thermal conductivity allows graphene film (GF) to disperse heat efficiently from heat sources. Most importantly, the comfortable, lightweight and compact features promote the application of GFs in comfortable light-emitting devices. Shielding composites have great application prospects in lightweight, electromagnetic composites, portable and wearable electronic devices due to their excellent EMI shielding performance and thermal stability, as well as enhanced thermal conductivities.[108,109] Cross-plane scattering of low-frequency phonons, which increases the convection of the graphene layer film bond plane by overcoming the longer flexural photon life.[110] These findings offer proof that the graphene layer film dropped on the FGO surface offers an extremely desirable medium for heat and energy control progress.[111]

Thermal Modelling

Different techniques are used for thermal modelling, in which each process yields different results, often with common materials. It also explains the core and important role of graphene materials and other 2D materials for practical use

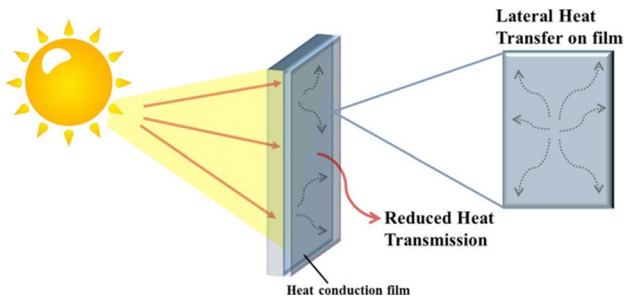

Fig. 7 Applications of graphene film as a heat spreader in a smart window. Reprinted from Ref. 112, under the terms of the Creative Commons Attribution License CC-BY 4.0, https://creativecommons.org/licenses/by/4.0/.

in micro thickness measurements.[113] Here is a description of the state-of-the-art thermal measurement procedures used with graphene structures and other 2D graphene materials.

Thermal Bridge

The time period of heat conduction of nanotubes or nanowires is restrained in the arrangement of palette or packages using one heater and dual sensors method and the restrained thermal conductivity is not inherent owing to the conquered inter-tube sprinklings.[114] Multilayer electron-beam lithography was used to create micro-devices appropriate for heat calculation, deuce suspended microelectromechanical systems (MEMS) were developed and used to deactivate lower-dimensional patterns and detect temperature changes at microscale.[115] Done for the submission. This thermal bridge process is considered to be one of the most effective methods for calculating heat conduction and thermal power of carbon nanotubes, nanowires and 2D graphene materials.[116]

Platinum or gold resistive coil is prefabricated on top of separate SiNx membrane and beam, which serve as both heater (R_h) and temperature sensor which is dependent on the track of the distribution of heat. The suspended single-layer graphene heats the two layers and electrically separates them from the resistive coil.[117] The unit should be put in a room equipped with vacuum pump to provide pressure environment greater than 1×10^{-5} pa to remove circumstantial gas convection and thermal radiation between the layers. AC heater with a DC voltage bias is applied up to current usually from 100 nA. Any frequency a few thousand hertz frequencies and additional AC current sensor of the identical amplitude or frequency.[118] The DC current (I) is used to add microwatt heat to the heater and to increase its temperature (T_h) and AC current is used to test the resistance of R_h/R_s, which is T_h/T_s. Suitable for T_s later resistive coils can be used as temperature controllers. At a stable state, the heat conductivity of the film these and the suspended SiNx beams can be obtained from $\sigma_l = (Q_h + Q_l)/(\Delta T_h + \Delta T_s)$ and $\sigma_s = \Delta T_s \sigma_l /$

$(\Delta T_h - \Delta T_s)$, where Q_h, Q_l, ΔT_h, and ΔT_s and the heating tee heater connected to the above-mentioned heating capacity, the heating energy on the SiNx beam, Rh and the temperature rise.[119] The thermal conductivity of the film can be obtained by $K = L \times \sigma_s / S = L/(R \times S)$ where L, S and R are the sample volume, cross-section area and whole thermal resistance. The thermal bridge approach is widely used to calculate the thermal conductivity of suspended single-layer or multilayer 2D materials, including graphene, boron nitride, black phosphorus, transition-metal dichalcogenides, and so on, but there are numerous challenges. At higher temperature, the thermal stability is beneficial to the film surface and the film has excellent thermal stability which can help them perform better by preventing thermal decomposition. Thermally conductive composite films have excellent thermal properties and can be used in a high-temperature setting for an extended period of time.[120,121] For example, graphene and MoS_2 thermal conductivity works spontaneously at times, retaining internal thermal conductivity with hot debate and disagreement.[122]

EB Self-heating Method

The electron beam (EB) self-heating system delivers straight dimension of heat interaction resistance and hence of internal thermal conductivity. This procedure is updated on the basis of the current bond technique and the model is combined within the scanning electron microscope (SEM) compartment which improves the quantity.[123] In contrast to the thermal bridge process, Rh heat foundation acts as a temperature instrument, the binary layers are used as a temperature device and the electron stream of light is used as a heat source.[124] Figure 8 shows the cogeneration technique of energy storage systems. Electrical energy is produced by combined heat and power (CHP) plants, wind farms and other plants and thermal control demand are maintained by CHP plants. For calculations, the electron beam is perused laterally towards the extent of the model, throughout which time the energy storage system of the electrons is consumed and hence the resident space is heated.[125] The resident heat produced by the engrossed electrons streams to the dual layers and increases their temperature range. The calculated current resistance is applied from one layer to the heating area and where reflection loss (RL) is equal to heat resistance of the auxiliary beam, X is the detachment from the layer to H.

Pulsed Photothermal Reflectance

In the experimental setup of pulsed photosensitive thermal reflectance (PPR), the thermal conductivity (bulk or film) of the material is described by a thermal reflection technique in the nanosecond regime. Kiding et al. reported the

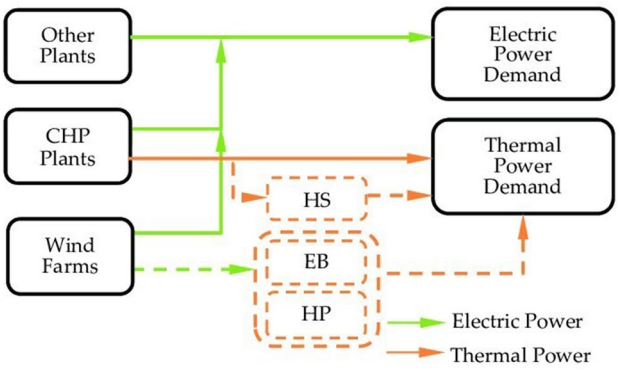

Fig. 8 Model of cogeneration system with energy storage. Reprinted from Ref. 126, under the terms of the Creative Commons Attribution License CC BY 4.0 licence, https://creativecommons.org/licenses/by/4.0/.

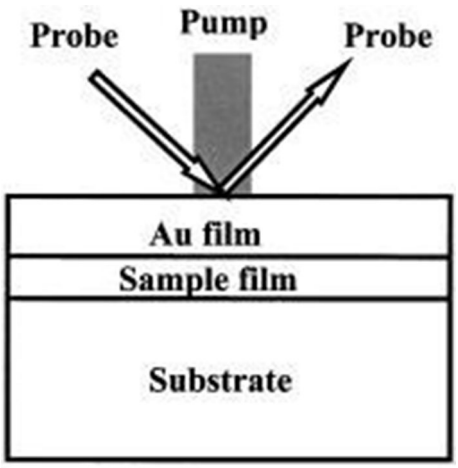

Fig. 9 Photothermal reflectance film measurement. Reprinted with permission from Ref. 130, Copyright 2004, AIP Publishing.

original method using PPR technologies to test the thermal conductivity of SiO_2 thin films.[127] Figure 9 shows the photothermal reflectance coating measurement. To increase the heat absorption, the gold layer evaporates above the surface. In this method, the sample surface is kept at the first and the surface temperature of the sample increases rapidly and then relaxes over time. This leads to a temperature excursion profile, which depends on the thermal properties of the underlying films and the thermal resistance between the layers. The technology is an optical and non-contact system containing a laser impel and a laser probe.[128] Prior to the calculation of thermal conductivity, the metallic layer, ideally gold, is dropped on the top of the film surface with the intention of capturing temperature captivation and external temperature through thermal reflective technology.[129]

Resistance Dependence on Temperature

The deferred model is impassioned by applying an alternating current (AC) and a direct current (DC) over the film and the sample temperature is determined by the resistance of the sample temperature. In this circumstance, the constant of resistance of the film is also restrained.[131] The flick is suspended between two copper heat sinks and mounted in a void cavity, and the electrode is located in a four-point discrepancy conformation. The sample length with a width ratio of less than 0.1 can be sliced into bits.[132] The heat transfer with GF can also be regarded as a 1D heat transfer. In the AC system, a current frequency of RMS = 1 mA at 2000 Hz is added to the DC current model, which increases its temperature by heating. Then the tolerance of the sample to various DC values is sample (DC) = blank, obtained from rms where RMS is the primary sympathetic voltage drop and transversely the sample as restrained by the lock internal amplifier.[133] Table 2 presents the thermal measurement methods. Throughout the self-heating process of the sample, the modification in electric resistance is restrained and the overall heat increase is determined.[134] The heat conduction of the film is then achieved by means of the added Joule heating control and the resulting typical heat increase as the input of the average heat conduction case of a 3D graphene spray structure.[135,136]

Joule Heat

Nanomaterials such as graphene and CNT are temperature-dependent on the Joule heating effect. In this process, the suspended graphene film is active by DC application and the heat increase of the model is estimated by infrared radiation (IR). Heating setup and sketch of models for Joule throughout the dimension, the sample is deferred and connected to both electrodes.[137] The DC current is powered by the solid and the heat of the material varies evenly. The DC current is calibrated to the target material with a temperature increase of less than 10 °C in order to avoid radiation and convection losses. The volumetric heat output is uniform due to Joule heating, $Q = VI/(Lwt)$, where W, T and L are the distance, depth and measurement of the model, and V, I are voltage and current, correspondingly.[138] Due to the disparity in the heat volume and the heat sink of the target material, the heat travels laterally towards the film and reaches a stable state within a few microseconds after heating. Both tests were done in an airtight laboratory atmosphere to prevent the influence of air flow.[139] The temperature of the heat sink during calculation is held at a steady temperature of $T_{L/2} = T_{-L/2} = T_o$. The temperature profile of the goaled solid is proportionally disseminated with deference to the core of the target solid is disseminated correspondingly with respect to the centre of the model.[140] Figure 10 explains the Joule heating method around the CNT structures. Since the electrons mainly pass inside the polymer matrix via CNT, the Joule heating process takes place around CNTs initially, and it occurs gradually over the area of high temperature around the CNTs and in the whole composite.

The highest temperature was reached in the centre of the T_M sample. In view of the temperature at the advantage (T_0) and midpoint (T_M) of the sample, the thermal conductivity of the target material is described by the subsequent equation:

$$K = \mathrm{VIL}/2 \text{ over } 4 \text{ wt } \left(T_m - T_o\right) \tag{5}$$

where K is the thermal conductivity of the target material in the level. Thermal conductivity can be determined by calculating the temperature at the control and middle of the specimen with an IR meter, the voltage around the sample and the contemporary and measurement of the sample.[142] For example, Wang et al. used the Joule heating technique to calculate the thermal conductivity of better heat-conducting graphene adhesives, and the thermal conductivity of conductive adhesives with 3 wt.% graphene was 8 W m^{-1} K^{-1}. This is roughly four times the position conductive epoxy resin without graphene, with improved graphene picture and the temperature profile and conductive adhesive pattern.[143]

Laser Flash

Laser flash technology is a commonly used tool for calculating thermal deviations and thermal conductivity of constituents owing to certain essential characteristics such as great accuracy and duplicability, low dimensions and a well-defined test area.[144] Laser flash analysis defines thermal conductivity of aircraft by means of millimetre-thin aircraft

Table II Thermal measurement methods[136]

Fabrication method	Material geometry	Measurement	Advantages	Limitations
Thermal bridge	Single layer thin film	Thermal conductivity	High accuracy	Complex sample preparation
Electron beam heating	Multilayer membrane	Interfacial thermal resistance	Easy sample preparation	Difficult to fabricate clean
Scanning thermal microscope	Single layer thin film	Heat dissipation	Freedom in material size	Very difficult to measure heat conduction due to heat loss

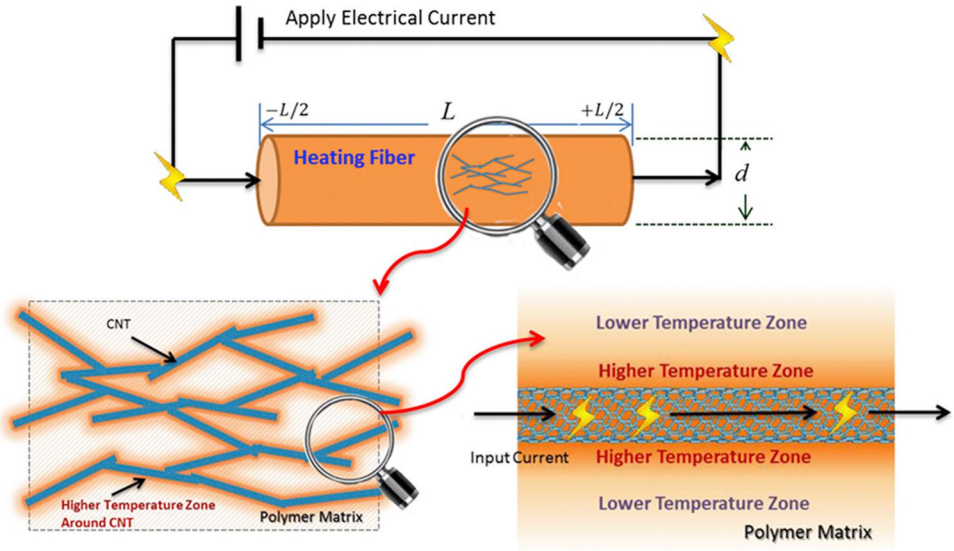

Fig. 10 Joule heating around CNTs. Reprinted with permission from Ref. 141, Copyright 2014, Elsevier.

versions. The minor surface of the model is first excited by a small laser pulse during measurement. The temperature difference that occurs on the top exterior of the film is then restrained by an infrared detector.[116] In its simplest adiabatic conformation, the thermal diffraction thickness of the film is related to the thickness of L and the maximum temperature increase of t50 is half the time. More complex models allow for correction due to small pulse duration and heat loss.[145] As long as the properties of all layers are understood in advance, it is also possible to calculate multilayer structures with contact resistance between three or two layers. Figure 11 describes the measurement of heat conduction using laser flash method. The laser-flash sample heats one of the surfaces with a small pulse, and the infrared detector measures the temperature rise over the other surface over time. From the temperature lifetime curve, the thermal diffusivity is calculated.[146] Such an uncontacted laser flash system has the benefit of eradicating the influence of connection heat resistance and is closely related to the high heat properties of the material.[147,150] In accumulation, the period determination of the participation optical maser and indicator has a durable outcome on the precision of the test outcomes.[148,151]

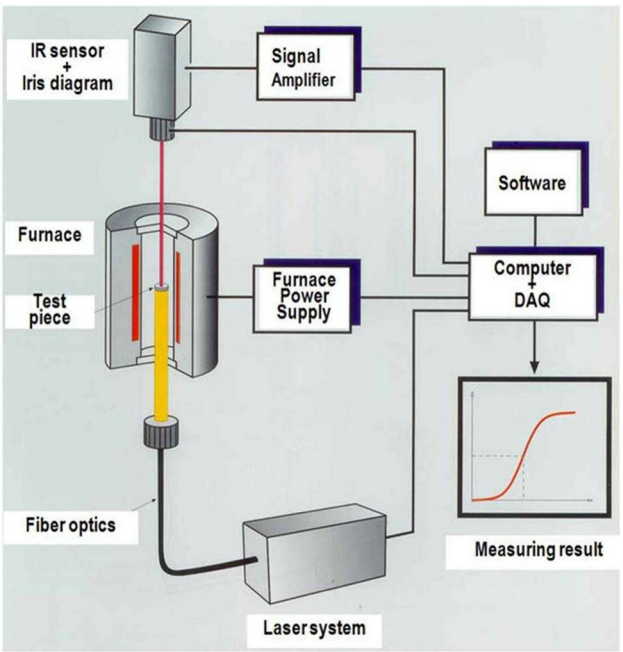

Fig. 11 Thermal diffusivity measurement system using the laser method. Reprinted from Ref. 149, under the terms of the Creative Commons CC-BY-NC-ND 4.0, https://creativecommons.org/licenses/by-nc-nd/4.0/.

Future Applications of Graphene Materials

Recently, some of the applications of graphene materials have been established for the use of graphene-based materials and other associated 2D materials for thermal management in consumer products. Graphene structures have been utilized to coat light-emitting diode (LED) strands, and graphene is reported to help dissipate heat in LED bulbs, thereby prolonging the generation and strengthening the performance of LEDs. Graphene-based materials of various thicknesses have been applied as heat spreader, with thermal conductivity of 3200 W m^{-1} K^{-1}. In addition, precipitously oriented graphene-based TIM materials can achieve thermal conductivity up to 1000 W m^{-1} K^{-1} direction of Z. Graphene-based materials have also been used as thermal paste, with thermal conductivity greater than 10 W m^{-1} K^{-1} reported. It seems that graphene can efficiently lower the temperature of the mounted film vision. In order to further

reduce the temperature, the efficiency of graphene film is required.

Conclusion

High-quality graphene materials and 2D materials play a major role in industrial applications. They have thus garnered considerable interest and led to significant advancements in the manufacture of graphene-related material for numerous applications in the science and engineering fields over the past few decades. The exceptional properties of graphene materials, especially for thermal management and energy storage control systems, have paved the way for thermal management applications in the scientific industries. This review article summarizes various graphene structures and graphene-based materials from science and engineering with a specific focus on thermal control systems due to their excellent structural and management properties. We are hopeful and confident that this will inspire further systematic studies and at the same time advance more marketable applications in this field, including materials such as alloy fillers, as well as the application of graphene polymer as heat repellents. This active technology has paved the way for the implementation of 2D thermal control materials in industry. It is our heartfelt expectation that this will encourage further research experiments while at the same time creating more commercial applications in this field.

Outlook

A large number of research articles and reviews report on the development of energy storage materials, and still many improvements are required. The literature study showed that nanostructure materials in two dimensions were produced in enormous amounts and that very work on three-dimensional materials. Future work should therefore focus on the development of such materials and slight changes to the structure that may improve the electrochemical characteristics. The materials with an excellent surface area and conductivity increased the specific capacity, rate capacity of the material enormously, and it must therefore be improved. Recently, a great deal of attention was paid to the scientist and technologist for new materials such as the metal-organic/inorganic frameworks. However, very few articles on metal-organic framework are being published and need more attention in the future. In general, the development of these materials will certainly improve the storage and stability, which are strongly required.

Funding This work is partially funded by Centre for Applied Research, Chennai Institute of Technology vide funding number is CIT/CAR/2021/003.

Conflict of interest The authors declare that they have no conflict of interest.

References

1. E. Pop, V. Varshney, and A.K. Roy, *MRS Bull.* 37, 1273 (2012).
2. H. Huang, Y. Xu, X. Zou, J. Wu, and W. Duan, *Phys. Rev. B* 87, 205415 (2013).
3. H. Malekpour, P. Ramnani, S. Srinivasan, G. Balasubramanian, D.L. Nika, A. Mulchandani, R.K. Lake, and A.A. Balandin, *Nano Scale* 8, 14608 (2016).
4. A.A. Balandin, *Nat. Mater.* 10, 569 (2011).
5. S.-C. Shiu, and J.-L. Tsai, *Compos. Part B Eng.* 56, 691 (2014).
6. J.D. Renteria, D.L. Nika, and A.A. Balandin, *Appl. Sci.* 4, 525 (2014).
7. Y. Xu, Z. Li, and W. Duan, *Small* 10, 2182 (2014).
8. J. Zhu, D. Yang, Z. Yin, Q. Yan, and H. Zhang, *Small* 10, 3480 (2014).
9. W. Choi, and J.-W. Lee eds., *Graphene: Synthesis and Applications*. (Boca Raton: CRC Press, 2011).
10. J.Y. Kim, J.-H. Lee, and J.C. Grossman, *ACS Nano* 6, 9050 (2012).
11. S.K. Singh, S. Goverapet -Srinivasan, and M. Neek-Amal, *Phys. Rev. B* 87, 104114 (2013).
12. S.R. Shin, Y.-C. Li, H.L. Jang, P. Khoshakhlagh, M. Akbari, A. Nasajpour, Y.S. Zhang, A. Tamayol, and A. Khademhosseini, *Adv. Drug Deliv. Rev.* 105, 255 (2016).
13. A. Savchenko, V. Cherkas, C. Liu, G.B. Braun, A. Kleschevnikov, Y.I. Miller, and E. Molokanova, *Sci. Adv.* 4, eaat0351 (2018).
14. X. Wang, G. Sun, P. Routh, D.-H. Kim, W. Huang, and P. Chen, *Chem. Soc. Rev.* 43, 7067 (2014).
15. Y.-T. Li, Y. Tian, M.-X. Sun, T. Tu, Z.-Y. Ju, G.-Y. Gou, Y.-F. Zhao, Z.Y. Yan, F. Wu, D. Xie, H. Tian, *Adv. Funct. Mater.* 30, 1903888 (2020).
16. R. Kumar, R. Singh, D. Hui, L. Feo, and F. Fraternali, *Compos. Part B Eng.* 134, 193 (2018).
17. C. Wu, L. Xia, P. Han, Xu. Mengchi, B. Fang, J. Wang, J. Chang, and Y. Xiao, *Carbon* 93, 116 (2015).
18. B.C. Thompson, E. Murray, and G.G. Wallace, *Adv. Mater.* 27, 7563 (2015).
19. Y. Liu, X. Dong, and P. Chen, *Chem. Soc. Rev.* 41, 2283 (2012).
20. S. Aznar-Cervantes, A. Pagán, J.G. Martínez, A. Bernabeu-Esclapez, T.F. Otero, L. Meseguer-Olmo, J.I. Paredes, and J.L. Cenis, *Mater. Sci. Eng. C* 79, 315 (2017).
21. Z. Guo, D. Zhang, and X.-G. Gong, *Appl. Phys. Lett.* 95, 163103 (2009).
22. H. Malekpour, K.-H. Chang, J.-C. Chen, C.-Y. Lu, D.L. Nika, K.S. Novoselov, and A.A. Balandin, *Nano Lett.* 14, 5155 (2014).
23. D.S. Ghosh, I. Calizo, D. Teweldebrhan, E.P. Pokatilov, D.L. Nika, A.A. Balandin, W. Bao, F. Miao, and C. Ning Lau, *Appl. Phys. Lett.* 92, 151911 (2008).
24. C. Faugeras, B. Faugeras, M. Orlita, M. Potemski, R.R. Nair, and A.K. Geim, *ACS Nano* 4, 1889 (2010).
25. D.L. Nika, S. Ghosh, E.P. Pokatilov, and A.A. Balandin, *Appl. Phys. Lett.* 94, 203103 (2009).
26. T.Y. Kim, C.-H. Park, and N. Marzari, *Nano Lett.* 16, 2439 (2016).
27. A. Alofi, and G.P. Srivastava, *Phys. Rev. B* 87, 115421 (2013).
28. B. Yuan, C. Bao, L. Song, N. Hong, K.M. Liew, and Y. Hu, *Chem. Eng. J.* 237, 411 (2014).

29. L. Burk, M. Gliem, F. Lais, F. Nutz, M. Retsch, and R. Mülhaupt, *Polymer* 10, 1088 (2018).
30. X. Wang, W. Xing, X. Feng, Yu. Bin, Lu. Hongdian, L. Song, and Hu. Yuan, *Chem. Eng. J.* 250, 214 (2014).
31. X. Mi, L. Zhong, F. Wei, L. Zeng, J. Zhang, D. Zhang, and Xu. Tiwen, *Polym. Test.* 76, 473 (2019).
32. X. Ye, P. Gong, J. Wang, H. Wang, S. Ren, and S. Yang, *Compos. Part A Appl. Sci. Manuf.* 75, 96 (2015).
33. X. Qiu, H. Cai, X. Fang, and J. Zheng, *Polym. Compos.* 39, 1105 (2018).
34. R. Wang, Wu. Lixin, D. Zhuo, J. Zhang, and Y. Zheng, *Ind. Eng. Chem. Res.* 57, 10967 (2018).
35. J. Yang, Y. Huang, Y. Lv, P. Zhao, Qi. Yang, and G. Li, *J. Mater. Chem. A* 1, 11184 (2013).
36. J. Yang, Yu. Peng, L.-S. Tang, R.-Y. Bao, Z.-Y. Liu, M.-B. Yang, and W. Yang, *Nanoscale* 9, 17704 (2017).
37. C. Bao, L. Song, C.A. Wilkie, B. Yuan, Y. Guo, Hu. Yuan, and X. Gong, *J. Mater. Chem.* 22, 16399 (2012).
38. D.C. Marcano, D.V. Kosynkin, J.M. Berlin, A. Sinitskii, Z. Sun, A. Slesarev, L.B. Alemany, Lu. Wei, and J.M. Tour, *ACS Nano* 4, 4806 (2010).
39. J. Du, and H.-M. Cheng, *Macromol. Chem. Phys.* 213, 1060 (2012).
40. X. Yang, S. Fan, Y. Li, Y. Guo, Y. Li, K. Ruan, S. Zhang, J. Zhang, J. Kong, and J. Gu, *Compos. Part A Appl. Sci. Manuf.* 128, 105670 (2020).
41. Y. Guo, K. Ruan, X. Shi, X. Yang, and J. Gu, *Compos. Sci. Technol.* 193, 108134 (2020).
42. M. Li, Z. Ali, X. Wei, L. Li, G. Song, X. Hou, H. Do, J.C. Greer, Z. Pan, C.T. Lin, N. Jiang, *Compos. Part B Eng.* 208, 108599 (2020).
43. Y. Guo, X. Yang, K. Ruan, J. Kong, M. Dong, J. Zhang, J. Gu, and Z. Guo, *ACS Appl. Mater. Interfaces* 11, 25465 (2019).
44. Y. Guo, K. Ruan, X. Yang, T. Ma, J. Kong, N. Wu, J. Zhang, J. Gu, and Z. Guo, *J. Mater Chem. C* 7, 7035 (2019).
45. Y. Liu, Lu. Jiangyin, and Y. Cui, *Car. Res. Con.* 3, 29 (2020).
46. L. Jiang, and Z. Fan, *Nanoscale* 6, 1922 (2014).
47. Z. Sun, S. Fang, and Y.H. Hu, *Chem. Rev.* 120, 10336 (2020).
48. S. Sayyar, D.L. Officer, and G.G. Wallace, *J. Mater. Chem. B* 5, 3462 (2017).
49. H. Gao, and H. Duan, *Biosens. Bioelectron.* 65, 404 (2015).
50. X. Cao, Z. Yin, and H. Zhang, *Energy Environ. Sci.* 7, 1850 (2014).
51. K.M. Yocham, C. Scott, K. Fujimoto, R. Brown, E. Tanasse, J.T. Oxford, T.J. Lujan, and D. Estrada, *Adv. Eng. Mater.* 20, 1800166 (2018).
52. F. Yavari, Z. Chen, A.V. Thomas, W. Ren, H.-M. Cheng, and N. Koratkar, *Sci. Rep.* 1, 1 (2011).
53. S. Yang, L. Chen, Mu. Lei, and P.-C. Ma, *J. Colloid Interface Sci.* 430, 337 (2014).
54. E. Krueger, A. Nicole Chang, D. Brown, J. Eixenberger, R. Brown, S. Rastegar, K.M. Yocham, K.D. Cantley, and D. Estrada, *ACS Biomater. Sci. Eng.* 2, 1234 (2016).
55. R. Lv, and M. Terrones, *Mater. Lett.* 78, 209 (2012).
56. J.C. Meyer, A.K. Geim, M.I. Katsnelson, K.S. Novoselov, T.J. Booth, and S. Roth, *Nature* 446, 60 (2007).
57. L. Sheng, T. Wei, Y. Liang, L. Jiang, Qu. Liangti, and Z. Fan, *Carbon* 120, 17 (2017).
58. N. Sezer, S.A. Khan, and M. Koç, *Energy Technol.* 8, 2000532 (2020).
59. N.-J. Song, C.-M. Chen, Lu. Chunxiang, Z. Liu, Q.-Q. Kong, and R. Cai, *J. Mater. Chem. A* 2, 16563 (2014).
60. N. Wang, S. Chen, A. Nkansah, C.C. Darmawan, L. Ye, and J. Liu. Highly thermally conductive and light weight copper/graphene film laminated composites for cooling applications, in *2018 19th (ICEPT)* (IEEE, 2018), p. 1588.
61. G. Xin, H. Sun, T. Hu, H.R. Fard, X. Sun, N. Koratkar, T. Borca-Tasciuc, and J. Lian, *Adv. Mater.* 26, 4521 (2014).
62. B. Shen, W. Zhai, and W. Zheng, *Adv. Funct. Mater.* 24, 4542 (2014).
63. C. Teng, D. Xie, J. Wang, Z. Yang, G. Ren, and Y. Zhu, *Adv. Funct. Mater.* 27, 1700240 (2017).
64. C. Melis, G. Barbarino, and L. Colombo, *Phys. Rev. B* 92, 245408 (2015).
65. Y. Hong, C. Zhu, M. Ju, J. Zhang, and X.C. Zeng, *Phys. Chem. Chem. Phys.* 19, 6554 (2017).
66. A. Verma, R. Kumar, and A. Parashar, *Phys. Chem. Chem. Phys.* 21, 6229 (2019).
67. H.S. Ryu, H.-S. Kim, D. Kim, S.J. Lee, W. Choi, S.J. Kwon, J.-H. Han, and E.-S. Cho, *Micromachines* 11, 821 (2020).
68. D.N. Luta, An energy management system for a hybrid reversible fuel cell/supercapacitor in a 100% renewable power system. PhD diss., Cape Peninsula University of Technology (2019).
69. A.G. Marrani, A. Motta, R. Schrebler, R. Zanoni, and E.A. Dalchiele, *Electrochim. Acta* 304, 231 (2019).
70. T. Cowen, K. Karim, and S. Piletsky, *Anal. Chim. Acta* 936, 62 (2016).
71. R.-C. Zhang, D. Sun, Lu. Ai, S. Askari, M. Macias-Montero, P. Joseph, D. Dixon, K. Ostrikov, P. Maguire, and D. Mariotti, *ACS Appl. Mater. Interfaces* 8, 13567 (2016).
72. R.-C. Zhang, D. Sun, A. Lu, S. Askari, M. Macias-Montero, P. Joseph, D. Dixon, K. Ostrikov, P. Maguire, and D. Mariotti. *Polymer Nanocomposites with Enhanced Thermal Transport Performance* (2016).
73. R.R. Guimaraes, J.M. Gonçalves, O. Björneholm, C. Moyses Araujo, A. N. de Brito, and K. Araki. Single-atom electrocatalysts for water splitting, in *Meth. for Electrocatalysis* (Springer, Cham, 2020), pp. 67–111.
74. A.G. Fedorov, C. Green, and Y. Joshi. Devices including composite thermal capacitors. U.S. Patent 8,710,625, issued April 29, 2014.
75. S. Ghosh, V. Gueskine, M. Berggren, and I.V. Zozoulenko, *J. Phys. Chem. C* 123, 15467 (2019).
76. D. Han, X. Wang, W. Ding, Y. Chen, J. Zhang, G. Xin, and L. Cheng, *Nanotechnolgy* 30, 075403 (2018).
77. X. Liu, G. Zhang, and Y.-W. Zhang, *Nano Lett.* 16, 4954 (2016).
78. J. Zhang, Y. Hong, M. Liu, Y. Yue, Q. Xiong, and G. Lorenzini, *Int. J. Heat Mass Transf.* 104, 871 (2017).
79. B.-Y. Cao, J.-H. Zou, G.-J. Hu, and G.-X. Cao, *Appl. Phys. Lett.* 112, 041603 (2018).
80. B. Mortazavi, Y. Rémond, S. Ahzi, and V. Toniazzo, *Comput. Mater. Sci.* 53, 298 (2012).
81. A. Morelos-Gomez, R. Cruz-Silva, H. Muramatsu, J. Ortiz-Medina, T. Araki, T. Fukuyo, S. Tejima, K. Takeuchi, T. Hayashi, M. Terrones, M. Endo, *Nat. Nanotechnol.* 12, 1083 (2017).
82. Y. Qian, X. Zhao, Q. Han, W. Chen, H. Li, and W. Yuan, *Nat. Commun.* 9, 1 (2018).
83. A. Chih, A. Ansón-Casaos, and J.A. Puértolas, *Tribol. Int.* 116, 295 (2017).
84. A. Amiri, G. Ahmadi, M. Shanbedi, M. Savari, S.N. Kazi, and B.T. Chew, *Sci. Rep.* 5, 17503 (2015).
85. S. Chatterjee, R. Carter, L. Oakes, W.R. Erwin, R. Bardhan, and C.L. Pint, *J. Phys. Chem. C* 118, 10893 (2014).
86. Y. Qu, J. Wu, Y. Yang, Y. Zhang, Y. Liang, H. El Dirani, R. Crochemore, P. Demongodinc, C. Sciancalepore, C. Grillet, C. Monat, *Adv. Opt. Mater.* 8, 1048 (2020).
87. M. Sang, J. Shin, K. Kim, and K.J. Yu, *Nanomaterials* 9, 374 (2019).
88. P.-C. Lin, S. Lin, P.C. Wang, and R. Sridhar, *Biotechnol. Adv.* 32, 711 (2014).
89. K. Qiao, S. Guo, Y. Zheng, Xu. Xuetao, H. Meng, J. Peng, Z. Fang, and Y. Xie, *Mater. Sci. Eng. C* 93, 853 (2018).

90. M.-l Zhao, X.-q Liu, Ye. Cao, X.-F. Li, D.-J. Li, X.-L. Sun, Gu. Han-qing, and R.-X. Wan, *Sci. Rep.* 6, 37112 (2016).
91. J. Xu, T. Cui, T. Hirtz, Y. Qiao, X. Li, F. Zhong, X. Han, Yi. Yang, S. Zhang, and T.-L. Ren, *ACS Appl. Mater. Interfaces* 12, 18375 (2020).
92. P. Suvarnaphaet, and S. Pechprasarn, *Sensors* 17, 2161 (2017).
93. S. Herekar, Systems, methods, and kits to reduce surface heating during tissue treatment. U.S. Patent Application 15/896,886, filed June 28, 2018.
94. H. Zhao, R. Ding, X. Zhao, Y. Li, Qu. Liangliang, H. Pei, L. Yildirimer, Wu. Zhengwei, and W. Zhang, *Drug Discov. Today* 22, 1302 (2017).
95. T. Das, B.K. Sharma, A.K. Katiyar, and J.-H. Ahn, *J. Semicond.* 39, 011007 (2018).
96. M. Ioniţă, G.M. Vlăsceanu, A.A. Watzlawek, S.I. Voicu, J.S. Burns, and H. Iovu, *Compos. Part B Eng.* 121, 34 (2017).
97. T. Kitao, M.W.A. MacLean, K. Nakata, M. Takayanagi, M. Nagaoka, and T. Uemura, *J. Am. Chem. Soc.* 142, 5509 (2020).
98. D.Q. McNerny, B. Viswanath, D. Copic, F.R. Laye, C. Prohoda, A.C. Brieland-Shoultz, E.S. Polsen, N.T. Dee, V.S. Veerasamy, and A. John Hart, *Sci. Rep.* 4, 1 (2014).
99. A. Nourbakhsh, M. Heyns, and S. De Gendt. Graphene based field effect transistor. U.S. Patent 9,184,270, issued November 10, 2015.
100. S. Wang, L. Gai, J. Zhou, H. Jiang, Y. Sun, and H. Zhang, *J. Phys. Chem. C* 119, 3881 (2015).
101. Y. Yang, L.-I. Huang, Y. Fukuyama, F.-H. Liu, M.A. Real, P. Barbara, C.-T. Liang, D.B. Newell, and R.E. Elmquist, *Small* 11, 90 (2015).
102. Y. Chen, X. Hou, R. Kang, Y. Liang, L. Guo, W. Dai, K. Nishimura, C.-T. Lin, N. Jiang, and Yu. Jinhong, *J. Mater. Chem. C* 6, 12739 (2018).
103. G.U. Kumar, K. Soni, S. Suresh, K. Ghosh, M.R. Thansekhar, and P. Dinesh-Babu, *Exp. Therm. Fluid Sci.* 96, 493 (2018).
104. F.J. Sonia, M. Aslam, and A. Mukhopadhyay, *Carbon* 156, 130 (2020).
105. A. Jaikumar, S.G. Kandlikar, and A. Gupta, *Heat Transf. Eng.* 38, 1274 (2017).
106. C. Tan, Z. Dong, Y. Li, H. Zhao, X. Huang, Z. Zhou, J.-W. Jiang, Y.Z. Long, P. Jiang, T.Y. Zhang, B. Sun, *Nat. Commun.* 11, 1 (2020).
107. S.G. Prolongo, O. Redondo, M. Campo, and A. Ureña, *J. Coat. Technol. Res.* 16, 491 (2019).
108. P. Song, B. Liu, C. Liang, K. Ruan, H. Qiu, Z. Ma, Y. Guo, and Gu. Junwei, *Nano-Micro Lett.* 13, 1 (2021).
109. L. Wang, X. Shi, J. Zhang, Y. Zhang, and Gu. Junwei, *J. Mater. Sci. Technol.* 52, 119 (2020).
110. H. Rho, Y.S. Jang, S. Kim, S. Bae, T.-W. Kim, D.S. Lee, J.-S. Ha, and S.H. Lee, *Nanoscale* 9, 7565 (2017).
111. J. Alizadeh, and M.K. Moraveji, *Int. Commun. Heat Mass Transf.* 98, 31 (2018).
112. L.P. Yeo, T.D. Nguyen, H. Ling, Y. Lee, D. Mandler, S. Magdassi, and A.I.Y. Tok, *J. Sci. Adv. Mater. Dev.* 4, 252 (2019).
113. D.L. Nika, and A.A. Balandin, *Rep. Prog. Phys.* 80, 036502 (2017).
114. R. Gulfam, W. Zhu, L. Xu II., P.S. Cheema, G. Zhao, and Y. Deng, *Energy Convers. Manag.* 156, 25 (2018).
115. Y. Zhuang, K. Zheng, X. Cao, Q. Fan, G. Ye, Lu. Jiaxin, J. Zhang, and Y. Ma, *ACS Nano* 14, 11733 (2020).
116. D. Jeon, S.H. Kim, W. Choi, and C. Byon, *Int. J. Heat Mass Transf.* 132, 944 (2019).
117. X. Meng, H. Pan, C. Zhu, Z. Chen, Lu. Tao, Xu. Da, Y. Li, and S. Zhu, *ACS Appl. Mater. interfaces* 10, 22611 (2018).
118. H. Lu, J. Zhang, J. Luo, W. Gong, C. Li, Q. Li, K. Zhang, M. Hu, and Y. Yao, *Compos. Part A Appl. Sci. Manuf.* 102, 1 (2017).
119. S. Han, D. Wu, S. Li, F. Zhang, and X. Feng, *Adv. Mater.* 26, 849 (2014).
120. Y. Zhang, K. Ruan, X. Shi, H. Qiu, Y. Pan, Yi. Yan, and Gu. Junwei, *Carbon* 175, 271 (2021).
121. K. Ruan, Y. Guo, C. Lu, X. Shi, T. Ma, Y. Zhang, J. Kong, and J. Gu, *Research* (2021).
122. V. Dhinakaran, B. Stalin, M. Swapna Sai, J. Vairamuthu, and S. Marichamy, *Mater. Today Proc.* (2020).
123. A. Aiyiti, X. Bai, Wu. Jing, Xu. Xiangfan, and B. Li, *Sci. Bull.* 63, 452 (2018).
124. C. Zhang, Wu. Ming-Bang, Wu. Bai-Heng, J. Yang, and Xu. Zhi-Kang, *J. Mater. Chem. A* 6, 8880 (2018).
125. Y. Kim, T. Kim, J. Lee, Y.S. Choi, J. Moon, S.Y. Park, T.H. Lee, H.K. Park, S.A. Lee, M.S. Kwon, H.G. Byun, *Adv. Mater.* 33, 2004827 (2020).
126. Y. Yu, H. Chen, and L. Chen, *Energies* 11, 263 (2018).
127. H. Han, Y. Zhang, N. Wang, M.K. Samani, Y. Ni, Z.Y. Mijbil, M. Edwards, S. Xiong, K. Sääskilahti, M. Murugesan, Y. Fu, *Nat. Commun.* 7, 1 (2016).
128. X. Li, B. Huang, R. Li, H.-P. Zhang, W. Qin, Z. Qiao, Y. Liu, and G. Yang, *Small* 15, 1900338 (2019).
129. W. Bao, Z. Wang, and J. Zhu, *Int. J. Heat Mass Transf.* 147, 118950 (2020).
130. Y. Zhao, C. Zhu, S. Wang, J.Z. Tian, D.J. Yang, C.K. Chen, H. Cheng, and P. Hing, *J. Appl. Phys.* 96, 4563 (2004).
131. X.-K. Chen, J. Liu, Z.-H. Peng, D. Du, and K.-Q. Chen, *Appl. Phys. Lett.* 110, 091907 (2017).
132. Yu. Su, J.J. Li, and G.J. Weng, *Carbon* 137, 222 (2018).
133. Y. Hong, J. Zhang, and X.C. Zeng, *Phys. Chem. Chem. Phys.* 18, 24164 (2016).
134. B. Davaji, H.D. Cho, M. Malakoutian, J.-K. Lee, G. Panin, T.W. Kang, and C.H. Lee, *Sci. Rep.* 7, 1 (2017).
135. X.-K. Chen, Z.-X. Xie, W.-X. Zhou, L.-M. Tang, and K.-Q. Chen, *Carbon* 100, 492 (2016).
136. Y. Fu, J. Hansson, Y. Liu, S. Chen, A. Zehri, M. Samani, N. Wang, Y. Ni, Y. Zhang, Z.B. Zhang, Q. Wang, *2D Mater.* 7, 012001 (2019).
137. S.H. Noh, W. Eom, W.J. Lee, H. Park, S.B. Ambade, S.O. Kim, and T.H. Han, *Carbon* 142, 230 (2019).
138. Y. Liu, C. Liang, A. Wei, Y. Jiang, Q. Tian, Y. Wu, Z. Xu, Y. Li, F. Guo, Q. Yang, W. Gao, *Mater. Today Nano* 3, 1 (2018).
139. J. Ge, L.-A. Shi, Y.-C. Wang, H.-Y. Zhao, H.-B. Yao, Y.-B. Zhu, Ye. Zhang, H.-W. Zhu, Wu. Heng-An, and Yu. Shu-Hong, *Nat. Nanotechnol.* 12, 434 (2017).
140. Y. Liu, P. Li, F. Wang, W. Fang, Xu. Zhen, W. Gao, and C. Gao, *Carbon* 155, 462 (2019).
141. A.-T. Chien, S. Cho, Y. Joshi, and S. Kumar, *Polymer* 55, 6896 (2014).
142. R. Menzel, S. Barg, M. Miranda, D.B. Anthony, S.M. Bawaked, M. Mokhtar, S.A. Al-Thabaiti, S.N. Basahel, E. Saiz, and M.S.P. Shaffer, *Adv. Funct. Mater.* 25, 28 (2015).
143. A.-R. Raji, T. Varadhachary, K. Nan, T. Wang, J. Lin, Y. Ji, Yu. Bostjan Genorio, C.K. Zhu, and J.M. Tour, *ACS Appl. Mater. Interfaces* 8, 3551 (2016).
144. Y.-H. Zhao, Z.-K. Wu, and S.-L. Bai, *Int. J. Heat Mass Transf.* 101, 470 (2016).
145. Q.-Y. Li, W.-G. Ma, and X. Zhang, *Int. J. Heat Mass Transf.* 95, 956 (2016).
146. C.-Y. Lin, and W.-R. Liu, *J. Alloys Compd.* 790, 156 (2019).
147. P. Goli, H. Ning, X. Li, C.Y. Lu, K.S. Novoselov, and A.A. Balandin, *Nano Lett.* 14, 1497 (2014).

148. Y. Gan, M. Feng, and H. Zhan, *Appl. Phys. Lett.* 104, 171105 (2014).
149. W.S. Ryu, D.G. Park, U.S. Song, J.S. Park, and S.B. Ahn, *Nucl. Eng. Technol.* 45, 219 (2013).
150. Y.-L. Zhang, Li. Guo, H. Xia, Q.-D. Chen, J. Feng, and H.-B. Sun, *Adv. Opt. Mater.* 2, 10 (2014).
151. Q.-Y. Li, X. Zhang, and K. Takahashi, *Int. J. Heat Mass Transf.* 125, 1230 (2018).